JOURNAL OF MATERIALS SCIENCE 37 (2002) 871–877

Analytical modelling for sheet thermoforming of knitted fabric reinforced PMC

TEIK CHENG LIM, S. RAMAKRISHNA, HUAI MIN SHANG
Department of Mechanical Engineering, The National University of Singapore, Singapore 119260
E-mail: alan_tc_lim@yahoo.com

Knitted fabrics are known for their excellent stretching and draping properties due to their curved fabric architecture. In recent years knitted fabrics have been used as reinforcement network for polymer sheet thermo-processing. This paper describes a method for evaluating the product height, product profile and strain distribution of a flat polymer matrix sheet, reinforced with knitted fabric, undergoing the sheet thermoforming process. The availability of a knitted fabric reinforced PMC to stretch is proposed to be equal to the least ratio of curved loop length to its projected length. The product profile is then obtained from the availability of the material to stretch and the tool geometry involved. Finally a mapping scheme is proposed to evaluate the severity of deformation in terms of strain distribution. A reasonably good agreement is observed between the model and experimental results. An understanding of the severity of deformation distribution would shed light on the location of highest degree of deformation as well as its magnitude and should therefore assist the product designer in dealing with the thermoforming process of this new material.

1. Introduction

Thermoplastics have been shown to possess rapid processing and long shelf life qualities [1]. The extent to which a flat polymer sheet can be formed into products of single and double curvatures have been shown to be improved with unidirectional fibre reinforcement [2–6]. Due to weak properties in transverse direction for unidirectional laminas, laminates consisting of laminas with various fibre directions were used. Occurrence of ply-slip [7] in unidirectional fiber reinforced laminates during plunger penetration has been suppressed with the substitution of woven fabrics as reinforcement network [8–11]. Woven fabrics undergoing sheet thermoforming deform primarily by shearing, or the Trellis Effect (e.g. [12]). In recent years the use of knitted fabric reinforcement, especially plain weft-knits (Fig. 1), have been shown to significantly reduce the tendency of the composite sheet to wrinkle during thermoforming [13, 14]. This may well be attributed to the capability of the knitted fabrics to stretch by means of straightening of the fibre bundle loops.

The feasibility of knitted fabric reinforced polymers for sheet forming process leads to severity of deformation modelling, in terms of strain fields, by numerical method with due consideration to fibre bundle reorientation [15]. Updating of material properties in each element, according to strain states, and nodal coordinates have been shown to require tedious computations [16]. In addition, the transformation of a flat sheet into a shell of revolution demands various intermediate steps which affects the convergence, and hence accuracy, of the final numerical results. In this paper, an analytical method is proposed to predict the forming solutions based on the mesoscopic structure of the knitted fabric reinforcement and the tool geometry involved. The forming solutions are referred hereto as the final profile of the formed sheet and the severity of deformation. The severity of deformation is described herein as strain distribution.

2. Formulation

Consider a sheet formed composite profile as shown in Fig. 2. The composite sheet drapes around the tool surfaces such that the uncontacted portion of the sheet takes a conical shape and the contacted portion of the sheet takes after the tool profile. The sections O′, A′, B′, C′, D′ and E′ on the deformed sheet originate from the sections O, A, B, C, D and E respectively on the undeformed circular flat sheet. The draping assumptions lead to the contact angle, β, as [17, 18]

$$\beta = \sin^{-1}\frac{-b-\sqrt{b^2-4ac}}{2a} \quad \text{for} \quad H \le (R_n + R_s) \tag{1}$$

and

$$\beta = \sin^{-1}\frac{-b+\sqrt{b^2-4ac}}{2a} \quad \text{for} \quad H \ge (R_n + R_s) \tag{2}$$

where $a = [(R_t + R_s) - (R_p - R_n)]^2 + [H - (R_n + R_s)]^2$, $b = -2[(R_t + R_s) - (R_p - R_n)](R_n + R_s)$ and $c =$

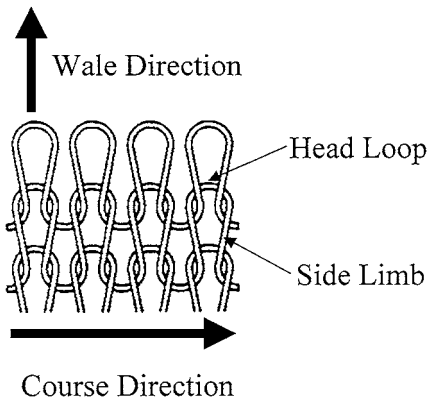

Figure 1 A plain weft-knit mesoscopic structure.

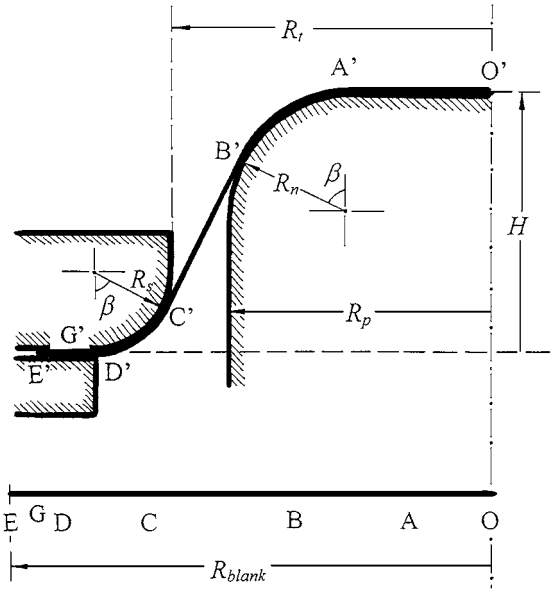

Figure 2 Section mapping profile of a thermoformed sheet.

$H[2(R_n + R_s) - H]$. Let h be the height of any section of the formed sheet at a radial distance r from the axis, then

$$h = H \quad \text{for} \quad 0 \le r \le (R_p - R_n), \tag{3}$$

$$h = H - R_n\left[1 - \cos\left(\sin^{-1}\frac{r - (R_p - R_n)}{R_n}\right)\right]$$
$$\text{for} \quad (R_p - R_n) \le r \le [R_p - R_n(1 - \sin\beta)], \tag{4}$$

$$h = R_s(1 - \cos\beta - \sin\beta\tan\beta) + [(R_t - R_s) - r]\tan\beta$$
$$\text{for} \quad [R_p - R_n(1 - \sin\beta)] \le r \le [R_t + R_s(1 - \sin\beta)], \tag{5}$$

$$h = R_s\left[1 - \cos\left(\sin^{-1}\frac{(R_t + R_s) - r}{R_s}\right)\right]$$
$$\text{for} \quad [R_t + R_s(1 - \sin\beta)] \le r \le (R_t + R_s) \tag{6}$$

and

$$h = 0 \quad \text{for} \quad (R_t + R_s) \le r \le R_{blank}. \tag{7}$$

Since $h = h(R_t, R_s, R_p, R_n, H, \beta)$ and $\beta = \beta(R_t, R_s, R_p, R_n, H)$, therefore the basic parameters of interest are the tool geometry and the product height. The depth of plunger penetration, which gives the product height, can be obtained from the availability of the knitted fabric composite to deform. Deformation of knitted fabric composite has been identified from the following three modes: (a) straightening of the curved fabric yarn, (b) slippage between overlapping yarns, and (c) fibre extension.

The foregoing formulation for the depth of plunger penetration considers only the first mode of deformation. Consider an arbitrarily curved loop of length $l(H)$ with a projection of $l_p(H)$ along the meridian of the tool at a plunger penetration of H, which correspond to a meridional length of $S(H)$. Incrementing the plunger penetration by ΔH gives a new length $l(H + \Delta H)$ and its projection $l_p(H + \Delta H)$ corresponding to a new product height $(H + \Delta H)$ and meridional length $S(H + \Delta H)$. Assuming no fiber extension, $l(H) = l(H + \Delta H)$, we have the incremental ratio of the projected length after the incremental plunger advancement to that before its movement as

$$\mathrm{d}\lambda = \frac{l_p(H + \Delta H)}{l_p(H)}. \tag{8}$$

Taking full straightening from zero product height to its current height gives

$$\lambda = \frac{l_p(H)}{l_p(0)} = \frac{l}{l_p} \tag{9}$$

where the initial yarn loop projection lengthens to l, equal to its curved length. Extending Equation 9 to the knitted fabric geometry given in Fig. 3 gives the potential of stretching in the course and wale directions as $\lambda_C = (l_H / l_{PH})$ and $\lambda_W = (l_S / l_{PS})$ respectively. l_H and l_S refer to the length of the head loop and side limb with l_{PH} and l_{PS} being the corresponding projected lengths along the course and wale axes respectively. In biaxial stretching, the lower of the two stretching potentials becomes the constricting factor. Therefore the stretching index can be set as $\lambda = \lambda_C$ if $\lambda_C \le \lambda_W$ or $\lambda = \lambda_W$ if $\lambda_C \ge \lambda_W$.

Perusal to Fig. 2 gives the ratio of the ratio of product meridional length at its current height $S(H)$ to that before deformation $S(0)$ as

$$\left[\frac{S(H)}{S(0)}\right]_1 = \frac{(R_p - R_n) + (R_n + R_s)\beta}{r_D} + \frac{H - (R_n + R_s)(1 - \cos\beta)}{r_D \sin\beta} \tag{10}$$

for the shell portion indicated by OABCD and

$$\left[\frac{S(H)}{S(0)}\right]_2 = \frac{r_{E'} - (R_t + R_s)}{R_{blank} - r_D} \tag{11}$$

for the flange portion indicated by the mapping of DE to D′E′. Equating the ratio of meridional stretching to that of the stretching potential

$$\left[\frac{S(H)}{S(0)}\right]_i = \lambda \quad \text{for} \quad i = 1 \tag{12}$$

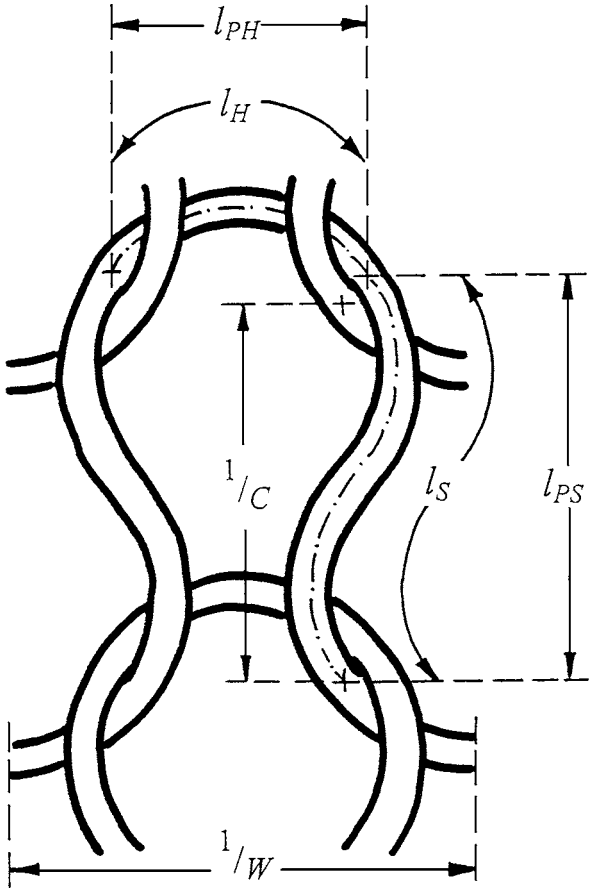

Figure 3 Geometrical parameters of a plain weft-knit.

gives the product height, which leads to the predicted product profile for both stretch forming and deep drawing processes.

The expressions given by Equations 10 and 11 can be simplified according to specific processes by first considering an arbitrary section G located between D and E which draws radially inward to G′ located between D′ and E′ as shown in Fig. 2. Consider a slight draw-in of G′ during a plunger penetration from $H = H$ to $H = (H + \Delta H)$, then the incremental draw-in experienced by section G′ is $\mathrm{d}\Psi = -(\mathrm{d}A_{OG'}/A_{OG'})$ where $A_{OG'}$ is the current projected circular area to the product base. The presence of negative sign ensures a positive value for draw-in during contraction of the projected area. The total draw-in for section G for large deformation can then be integrated to give $\Psi = 2\ln(r_G/r_{G'})$ where r_G and $r_{G'}$ refer to the initial and final radii respectively of the arbitrary section G. For convenience only the inner (Ψ_1) and outer (Ψ_2) draw-in

$$\Psi_1 = 2\ln\frac{r_D}{r_{D'}} = 2\ln\frac{r_D}{R_t + R_s} \tag{13}$$

and

$$\Psi_2 = 2\ln\frac{r_E}{r_{E'}} = 2\ln\frac{R_{blank}}{r_{E'}} \tag{14}$$

are defined to correspond to draw-in of section D arriving at the die throat and radial slippage at the blank rim, E, respectively. Substituting r_D from Equation 13 and $r_{E'}$ from Equation 14 into Equations 10 and 11 gives

$$\left[\frac{S(H)}{S(0)}\right]_1 = \frac{(R_p - R_n) + (R_n + R_s)\beta}{(R_t + R_s)\mathrm{e}^{\frac{\Psi_1}{2}}} + \frac{H - (R_n + R_s)(1 - \cos\beta)}{(R_t + R_s)\mathrm{e}^{\frac{\Psi_1}{2}}\sin\beta} \tag{15}$$

and

$$\left[\frac{S(H)}{S(0)}\right]_2 = \frac{R_{blank}\mathrm{e}^{-\frac{\Psi_2}{2}} - (R_t + R_s)}{R_{blank} - (R_t + R_s)\mathrm{e}^{\frac{\Psi_1}{2}}}. \tag{16}$$

For the special case of pure stretch forming the flange remains stationary throughout the event of plunger penetration such that formation of the shell is attained solely by stretching of the unclamped portion. Thus substituting

$$\Psi_i = 0 \quad \text{for} \quad i = 1, 2 \tag{17}$$

gives rise to

$$\left[\frac{S(H)}{S(0)}\right]_1 = \frac{(R_p - R_n) + (R_n + R_s)\beta}{(R_t + R_s)} + \frac{H - (R_n + R_s)(1 - \cos\beta)}{(R_t + R_s)\sin\beta} \tag{18}$$

and

$$\left[\frac{S(H)}{S(0)}\right]_2 = 1. \tag{19}$$

For the special case of full deep drawing, the flange completely draws radially inward into the die throat to form the cup wall. Therefore substituting

$$\Psi_i = 2\ln\frac{R_{blank}}{R_t + R_s} \quad \text{for} \quad i = 1, 2 \tag{20}$$

leads to

$$\left[\frac{S(H)}{S(0)}\right]_1 = \frac{(R_p - R_n) + (R_n + R_s)\beta}{R_{blank}} + \frac{H - (R_n + R_s)(1 - \cos\beta)}{R_{blank}\sin\beta} \tag{21}$$

with $[\frac{S(H)}{S(0)}]_2$ being non-existent due to the fully drawn condition.

The relative absence of localised meridional strain for knitted fabric reinforced thermoplastic sheets undergoing forming as compared to pure thermoplastic sheets, as shown in Fig. 4 suggests that:

(a) An incremental straightening of yarns, and hence material stiffening through geometrical alteration, at a certain unit cell of the composite sheet shifts the next incremental yarn straightening to the neighbouring representative volume element,

(b) Sliding between the composite sheet with the plunger surface occurs, albeit the presence of friction, to pave way for (a) to take place, and

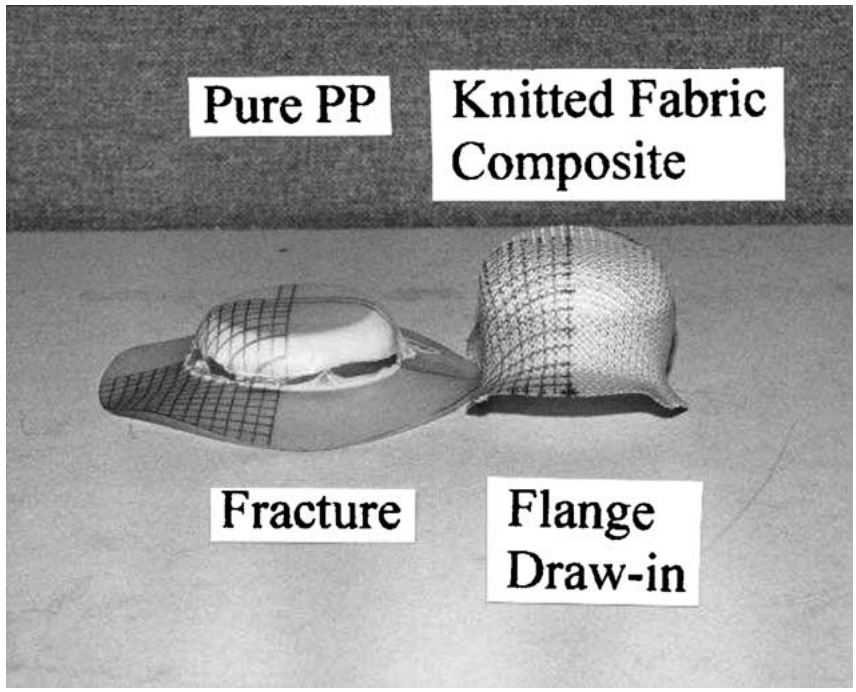

Figure 4 Comparison between a sheet formed pure PP and a knitted fabric reinforced PP [14].

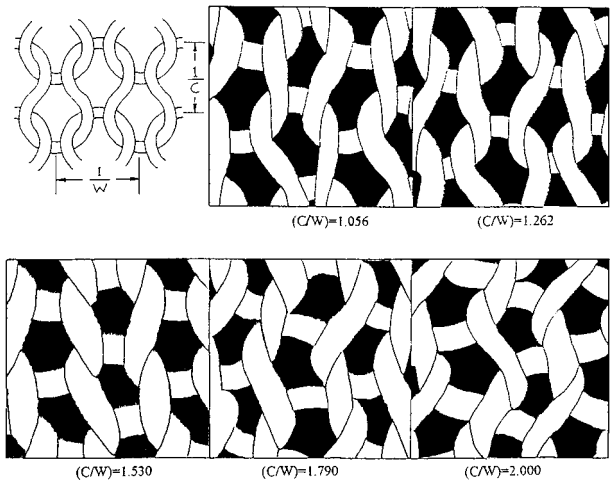

Figure 5 Yarn structure under various pre-stretching.

(c) Occurrence of fiber bundle slippage at the cross-over locations and fiber extension, in addition to (a), contribute to any deviation of meridional strain along the product meridian.

Consider the case of deformation by yarn straightening and insignificant friction, i.e. (a) and (b), while neglecting (c), we let the averaged meridional stretching along the shell meridian and flange radius be piecewise uniformly distributed, but can be different for both portions.
Thus

$$\left(\frac{\mathrm{d}s}{\mathrm{d}r_0}\right)_1 = \left[\frac{S(H)}{S(0)}\right]_1 = \left(\frac{\mathrm{d}s}{\mathrm{d}r_0}\right)_{SF} \mathrm{e}^{-\frac{\Psi_1}{2}} \tag{22}$$

and

$$\left(\frac{\mathrm{d}s}{\mathrm{d}r_0}\right)_2 = \left[\frac{S(H)}{S(0)}\right]_2 = \frac{R_{blank}\mathrm{e}^{-\frac{\Psi_2}{2}} - (R_t + R_s)}{R_{blank} - (R_t + R_s)\mathrm{e}^{\frac{\Psi_1}{2}}} \tag{23}$$

respectively according to Equations 15 and 16 where

$$\left(\frac{\mathrm{d}s}{\mathrm{d}r_0}\right)_{SF} = \frac{(R_p - R_n) + (R_n + R_s)\beta}{(R_t + R_s)} + \frac{H - (R_n + R_s)(1 - \cos\beta)}{(R_t + R_s)\sin\beta} \tag{24}$$

refers to the meridional stretching ratio for a pure stretch forming process. Perusal to Fig. 2 reveals five portions of the deformed sheet which drape accordingly to the axisymmetrical tool surfaces. A backward trace can be performed, based on the stretching criteria laid out in Equations 22 and 23, to give

$$r_A = (R_p - R_n)\left(\frac{\mathrm{d}s}{\mathrm{d}r_0}\right)_{SF}^{-1} \mathrm{e}^{\frac{\Psi_1}{2}}, \tag{25}$$

$$r_B = [(R_p - R_n) + R_n\beta]\left(\frac{\mathrm{d}s}{\mathrm{d}r_0}\right)_{SF}^{-1} \mathrm{e}^{\frac{\Psi_1}{2}}, \tag{26}$$

$$r_C = \left[(R_t + R_s) - R_s\beta\left(\frac{\mathrm{d}s}{\mathrm{d}r_0}\right)_{SF}^{-1}\right] \mathrm{e}^{\frac{\Psi_1}{2}}, \tag{27}$$

$$r_D = (R_t + R_s)\mathrm{e}^{\frac{\Psi_1}{2}} \tag{28}$$

and

$$r_E = R_{blank}. \tag{29}$$

By virtue of the same stretching criteria each section of radius r_0 on the original flat sheet can be forward traced to be mapped to the tool surfaces as

$$r = r_0\left(\frac{\mathrm{d}s}{\mathrm{d}r_0}\right)_{SF} \mathrm{e}^{-\frac{\Psi_1}{2}} \quad \text{for} \quad 0 \le r_0 \le r_A, \tag{30}$$

$$r = (R_p - R_n) + R_n \sin\left[\frac{r_0}{R_n}\left(\frac{\mathrm{d}s}{\mathrm{d}r_0}\right)_{SF} \mathrm{e}^{-\frac{\Psi_1}{2}} - \left(\frac{R_p}{R_n} - 1\right)\right] \quad \text{for} \quad r_A \le r_0 \le r_B, \tag{31}$$

$$r = (R_p - R_n) + R_n \sin\beta + \left[r_0\left(\frac{\mathrm{d}s}{\mathrm{d}r_0}\right)_{SF} \mathrm{e}^{-\frac{\Psi_1}{2}} - (R_p - R_n) - R_n\beta\right]\cos\beta \quad \text{for} \quad r_B \le r_0 \le r_C, \tag{32}$$

$$r = (R_t + R_s) - R_s \sin\left\{\frac{1}{R_s}\left[(R_t + R_s) - r_0 \mathrm{e}^{-\frac{\Psi_1}{2}}\right]\left(\frac{\mathrm{d}s}{\mathrm{d}r_0}\right)_{SF}\right\} \quad \text{for} \quad r_C \le r_0 \le r_D \tag{33}$$

and

$$r = (R_t + R_s) + \left[r_0 - (R_t + R_s)\mathrm{e}^{\frac{\Psi_1}{2}}\right] \times \left\{\frac{R_{blank}\mathrm{e}^{-\frac{\Psi_2}{2}} - (R_t + R_s)}{R_{blank} - (R_t + R_s)\mathrm{e}^{\frac{\Psi_1}{2}}}\right\} \quad \text{for} \quad r_D \le r_0 \le r_E. \tag{34}$$

The product profile, described by Equations 25 to 34, can be easily solved for two special cases. For the special case of pure stretch forming, the condition of no draw-in as specified by Equation 17 applies. For the special case of full deep drawn condition, the blank rim draws radially inward until the inner die edge such that Equation 20 prevails.

3. Processing of experimental data

For experimental verification, aramid (Kevlar®) fibre, in the form of plain weft-knitted structure, was used as textile reinforcement for polypropylene (PP) sheets. An investigation into the effect of fiber bundle structure, within the scope of plain weft-knitted fabric, is achieved by subjecting the fabrics to pre-stretching under various extent before undergoing compression moulding in the film stacking process. Details of specimen preparation, thermoforming processes and final grid coordinate measurement techniques are given elsewhere [13–15] and will not be repeated here. The effect of yarn geometry on the potential of the composites to be deformed was tested by their capability to be stretched by means of the stretch forming process. The usual hemispherical plunger was used in conformity to the stretch forming test [19]. Investigation into the influence of tool profile on the cup height and the resulting profile was made through the use of various plunger shapes in the deep drawing process. Table I presents the combination of tests. The ratios λ_W and λ_C were measured from photographically enlarged specimens (Fig. 5) using a flexible ruler. Results of the λ values give the theoretical product height given in Equations 10 to 12, which subsequently leads to the theoretical product profile described in Equations 3 to 7. As the theoretical product profile assumes axisymmetrical shape, coordinates along both the wale and course axes were measured for comparison.

In obtaining the experimental strain distribution, the coordinates measured along the wale (r_W, h_W) and course (r_C, h_C) axes were averaged as $r = (r_W + r_C)/2$ and $h = (h_W + h_C)/2$ so as to treat the product as being axisymmetric. Results of the product grid coordinates give the circumferential and thickness strain as described by

$$\varepsilon_\theta = \ln\frac{r}{r_0}, \tag{35}$$

and

$$\varepsilon_t = -(\varepsilon_\theta + \varepsilon_\phi) \tag{36}$$

respectively where

$$\varepsilon_\phi = \ln\frac{\mathrm{d}s}{\mathrm{d}r_0} \tag{37}$$

refers to the meridional strain.

4. Results and discussion

Results of measured and predicted product height are shown in Fig. 6 for stretch formed shells and deep drawn cups. For the case of stretch forming, higher pre-stretching tends to straighten the curved yarns, thereby decreasing the availability of the fabric to be further stretched. For the case of deep drawing, larger plunger nose radius (R_n) is associated with lesser shell area for

TABLE I Test combination for influence of yarn geometry and tool profile

Specimen	Pre-stretching direction	(C/W)	λ_W	λ_C	R_n (mm)	Process
1	Wale	1.056	1.062	1.4	37.5	S.F.
2	Wale	1.262	1.068	1.5	37.5	S.F.
3	No pre-stretching	1.530	1.080	1.3	37.5	S.F.
4	Course	1.790	1.070	1.4	37.5	S.F.
5	Course	2.000	1.052	1.4	37.5	S.F.
6	No pre-stretching	1.530	1.080	1.3	9.0	D.D.
7	No pre-stretching	1.530	1.080	1.3	16.0	D.D.
8	No pre-stretching	1.530	1.080	1.3	23.0	D.D.
9	No pre-stretching	1.530	1.080	1.3	30.0	D.D.
10	No pre-stretching	1.530	1.080	1.3	37.5	D.D.

S.F. = stretch forming, D.D. = deep drawing, $R_t = 40.0$ mm, $R_s = 6.0$ mm, $R_p = 37.5$ mm.

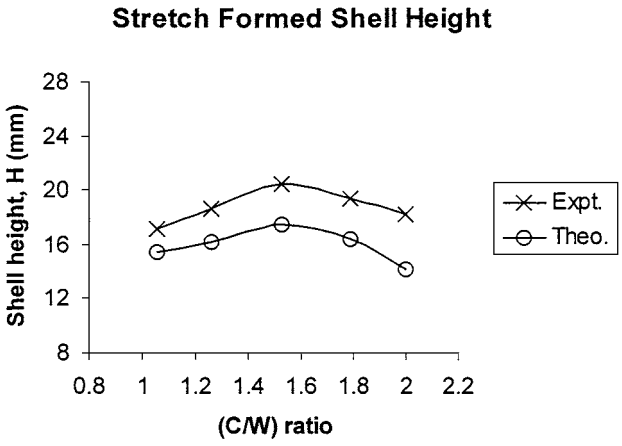

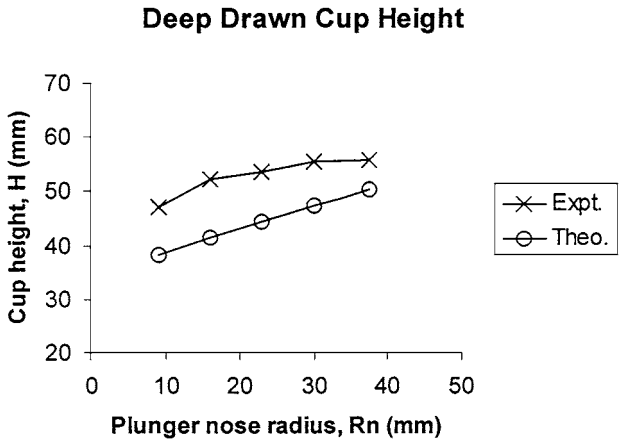

Figure 6 Product height for stretch formed shells and deep drawn cups.

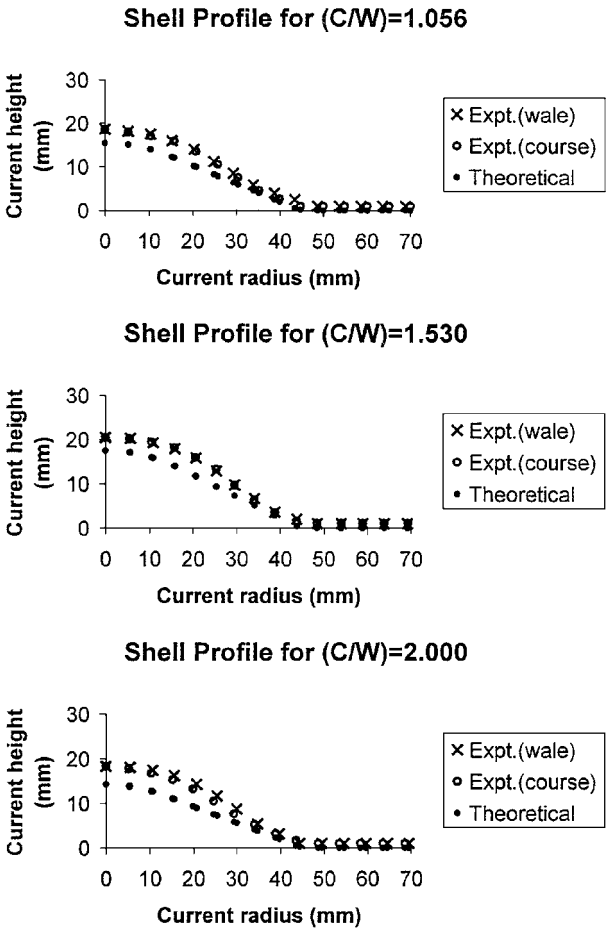

Figure 7 Stretch formed profile at $R_p = R_n = 37.5$ mm, $R_t = 40.0$ mm and $R_s = 6.0$ mm for various (C/W).

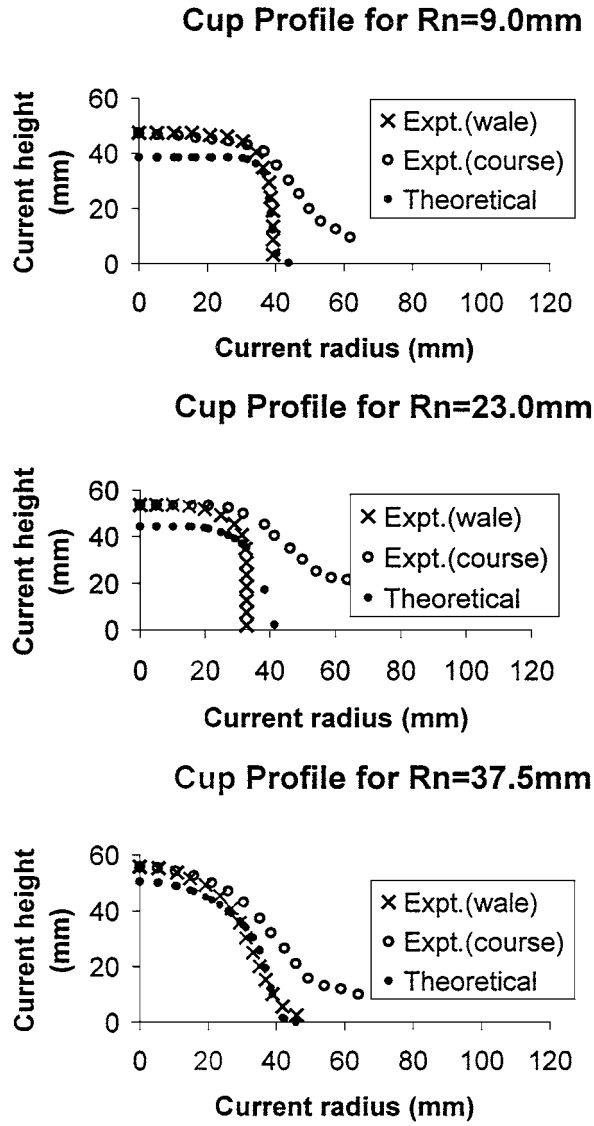

Figure 8 Deep drawn profile at $(C/W) = 1.53$, $R_p = 37.5$ mm, $R_t = 40.0$ mm and $R_s = 6.0$ mm for various R_n.

constant polar height (H). The corresponding demand for stretching thereby enables greater cup height to be attained. Fig. 7 presents the stretch formed profile for increasing (C/W) ratios. A slight underestimation of about 10% by the analytical model may well be due to the neglect of the remaining two modes of deformation-yarn slippage and fibre extension. Unlike the case of stretch forming, products formed from deep drawing leads to highly asymmetric shells, as shown in Fig. 8. The lower λ_W than λ_C leads to incomplete draw-in of the rim associated to the course axis when the wale axis is fully drawn. Springback of the course portion gives rise to warping.

The strain distributions shown in Fig. 9 correspond to the stretch-formed profile of Fig. 7. Since the clamped portion remains stationary, the central portion deforms by meridional strain, thus giving rise to positive circumferential strain and negative thickness strain. Unlike stretch forming, the clamped portion flows radially inward—leading to negative circumferential strain at the cup wall (outer portion) as shown in Fig. 10—for the case of deep drawing. Since the fabric structure limits the extent of meridional strain, the large negative circumferential strain leads to thickening by virtue of

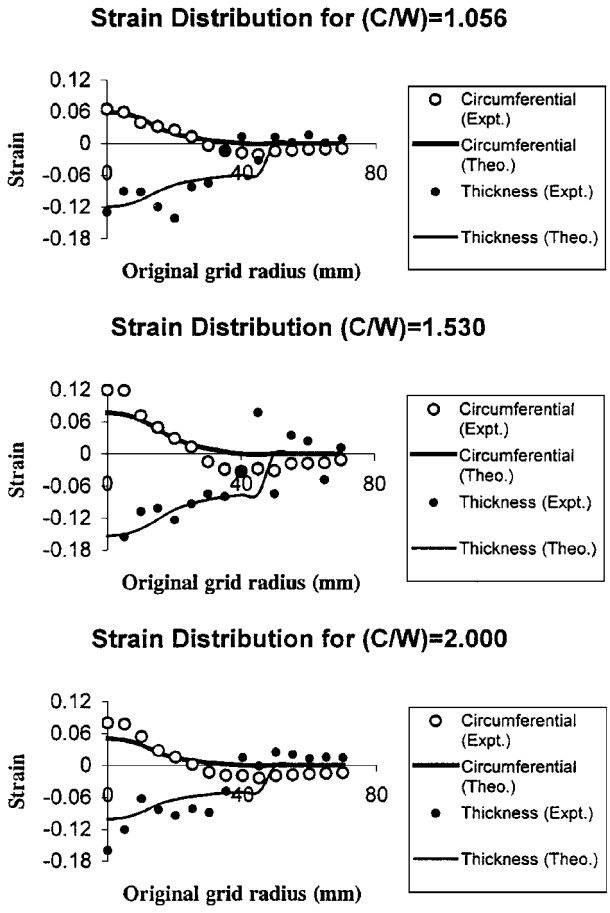

Figure 9 Stretch formed strain field at $R_p = R_n = 37.5$ mm, $R_t = 40.0$ mm and $R_s = 6.0$ mm for various (C/W).

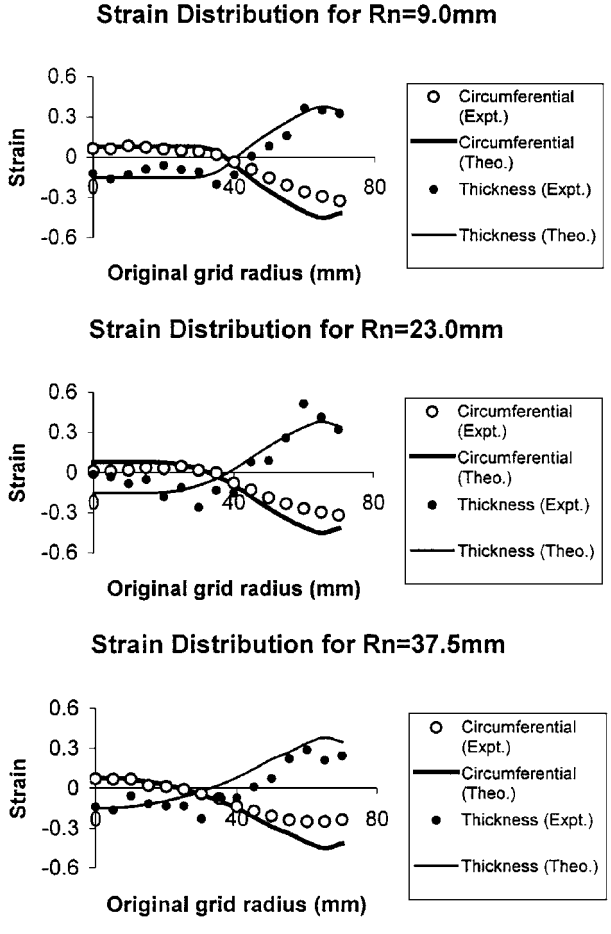

Figure 10 Deep drawn strain field at $(C/W) = 1.53$, $R_p = 37.5$ mm, $R_t = 40.0$ mm and $R_s = 6.0$ mm for various R_n.

material incompressibility. Albeit such discrepancies exist, the reasonably good agreement between the predicted and measured strain distribution suggests that straightening of the curved fiber bundle is the major mode of the composite sheet deformation.

5. Conclusions and suggestions

Prediction on the mode and severity of deformation has been made on the basis of material stretching availability. Plainly speaking, the mesoscopic structure of the knitted fabric reinforcement and the tool geometry determine the (a) depth of plunger penetration, and hence the product height, (b) product profile; and (c) the strain distribution throughout the entire sheet. The assumption of fiber bundle straightening as the potential of the curved fabric composite to deform may well be understood as the *supply* to which the tool geometry and plunger penetration set the *demand*. Though by-passing of the constitutive relations appears to be a deficiency rather than a merit to the present approach, the offer of a single-step calculation and closed-form solution leads to quick analysis for practical applications. An understanding of the severity of deformation distribution should assist the product and die designers in dealing with this new material undergoing thermoforming processes.

Consideration of fiber bundle slippage and its extension is expected to contribute towards higher accuracy to the prediction models, and is hence suggested to be incorporated in future work.

References

1. F. N. COGSWELL, *Compos. Manuf.* **2** (1991) 208.
2. T. G. ROGERS and A. C. PIPKIN, *J. Appl. Mech.* **38** (1971) 1047.
3. T. G. GUTOWSKI, D. HOULT, G. DILLON and J. GONZALEZ-ZUGASTI, *Compos. Manuf.* **2** (1991) 147.
4. C. M. O'BRADAIGH, G. B. McGUINESS and R. B. PIPES, *ibid.* **4** (1993) 67.
5. A. K. PICKETT, T. QUEKBORNER, P. DE LUCA and P. B. PIPES, *ibid.* **6** (1995) 237.
6. M. HOU, *Compos. Part A* **28** (1997) 695.
7. M. F. TALBOT and A. K. MILLER, *Polym. Compos.* **11** (1990) 387.
8. R. E. ROBERTSON, E. S. HSIUE and G. S. Y. YEH, *ibid.* **5** (1984) 191.
9. A. J. SMILEY and R. B. PIPES, *J. Thermoplast. Compos. Mater.* **1** (1988) 298.
10. L. YE and H. R. DAGHYANI, *Compos. Part A* **28** (1997) 869.
11. J. WANG, R. PATON and J. R. PAGE, *ibid.* **30** (1999) 757.
12. Y. NAKAMURA and T. OHATA, *Key Eng. Mater.* **137** (1998) 40.
13. T. C. LIM, S. RAMAKRISHNA and H. M. SHANG, *Mater. Sci. Res. Int.* **5** (1999) 57.
14. *Idem.*, *Compos. Part B* **30** (1999) 495.
15. T. C. LIM, M. FUJIHARA, M. ZAKO, S. RAMAKRISHNA and H. M. SHANG, *Sci. Eng. Compos. Mater.* **8** (1999) 113.
16. T. C. LIM, M. ZAKO, S. SAKATA and S. RAMAKRISHNA, *Adv. Compos. Lett.* **9** (2000) 257.
17. S. QIN, H. M. SHANG, C. J. TAY and J. MO, *J. Mater. Process. Technol.* **63** (1997) 117.
18. T. C. LIM, PhD thesis, The National University of Singapore (2000).
19. J. CHAKRABARTY, *Int. J. Mech Sci.* **12** (1970) 315.

Received 18 February 2000
and accepted 26 September 2001